



Correlation of Electrical Conductivity and Microstructure with the Band Gap of Oxysulfide Glass-Ceramics for Na-Ion Battery

PARAMJYOT KUMAR JHA^{1,*}, GOURAV SINGLA¹, SAVIDH KHAN² and PARDEEP KUMAR NAGPAL³

¹Department of Physics (UIS), Chandigarh University, Gharuan-140413, India

²Department of Physics, RIMT University, Mandi Gobindgarh, Fatehgarh Sahib-147301, India

³Department of Mechanical Engineering, I.K. Gujral Punjab Technical University, Kapurthala-144603, India

*Corresponding author: E-mail: paramjyotjha@gmail.com

Received: 28 January 2024;

Accepted: 5 April 2024;

Published online: 30 April 2024;

AJC-21625

In the present investigation, a glass-ceramics with the composition of $x\text{Na}_2\text{S} + (100-x)\text{P}_2\text{S}_5$, where $x = 40, 45, 50$ and 55 , were successfully synthesized by employing the melt-quenching method. Comprehensive characterization of the glass-ceramic samples was conducted using X-ray diffraction (XRD), UV-visible spectroscopy, impedance spectroscopy (IS) and field emission scanning electron microscopy (FE-SEM) techniques. The XRD analysis revealed the presence of three distinct phases, namely NaPO_3 , $\text{Na}_2\text{S}_2\text{O}_3$ and Na_3PS_4 , in all samples. Significantly, NaPO_3 and $\text{Na}_2\text{S}_2\text{O}_3$ exhibited an orthorhombic crystal structure, while Na_3PS_4 displayed a tetragonal crystal structure. The densities of the synthesized samples fell within the range of 2.24 to 2.35 g/cc, surpassing those of Li_2S -based solid electrolytes commonly used in portable devices. The band gap of the materials varied from 2.99 to 3.60 eV. Significantly, an inverse relationship between Na_2S content (modifier) and band gap was observed, indicating a decrease in band gaps with increasing Na_2S content. This phenomenon is beneficial for enhancing ionic conductivity. At ambient temperature, samples with x values of 50 and 55 demonstrated remarkable conductivity on the order of 10^{-4} S cm^{-1} . Overall, the synthesized glass ceramics exhibit promising features, such as higher density compared to conventional Li_2S -based solid electrolytes and favourable band gap values, suggesting their potential application in enhancing ionic conductivity for various electronic devices.

Keywords: Sulfide glass-ceramics, Solid electrolyte, Ionic conductivity, Na-ion battery.

INTRODUCTION

In recent years, the solid-state sodium-ion rechargeable batteries have gained wide attention due to abundant sodium sources, impressive energy densities reaching up to 760 Wh kg^{-1} and their applicability in distributed power systems for storing renewable energy [1-3]. Addressing safety concerns, all solid-state batteries leverage solid inorganic electrolytes instead of liquid organic electrolytes, mitigating issues such as leakage, volatilization and flammability [4,5]. To achieve high ionic conductivity, researchers are focusing on the development of sulfide-based glasses and glass-ceramics as solid electrolytes [6-8]. These materials exhibit high polarizabilities of sulfidions, enhancing ionic conductivity. Elevated temperatures during glass processing can lead to the formation of a high-temperature super-ionic phase within the glass matrix [9].

Tatumisago *et al.* [10] reported the stabilization of high temperature super-ionic phase $\alpha\text{-AgI}$ at room temperature within a glass matrix, resulting in an exceptionally high ionic conductivity of 10^{-1} S cm^{-1} . Nevertheless, the practical applications of silver iodide-based glasses are constrained by their electrochemical decomposition occurring at voltages exceeding 680 mV. To overcome this problem, recent studies [11,12] have reported new glass-ceramic solid electrolytes like $\text{Li}_3\text{P}_7\text{S}_{11}$ and $\text{Li}_{10}\text{GeP}_2\text{S}_{12}$ displaying impressive ionic conductivity. The $\text{Li}_2\text{S}-\text{P}_2\text{S}_5$ system-based solid electrolytes have exhibited excellent cycling and rate performances, making them suitable for all-solid-state lithium-ion secondary batteries [13,14]. However, the insufficiency of lithium may impact its future cost, prompting the exploration of sodium as an alternative material. The abundant availability and cost-effectiveness of sodium resources, sodium-ion batteries (SIBs) are recognized as a promising

alternative for the next-generation of large-scale electrical energy storage systems [15,16].

Hayashi *et al.* [17] developed a Na-sulfide glass-ceramic solid electrolyte, which feature a crystallized cubic Na_3PS_4 phase from the glassy state. This resulted in a significant room temperature ionic conductivity of $2 \times 10^{-4} \text{ S cm}^{-1}$. Additionally, Berbano *et al.* [18] explored glasses and glass-ceramics composed of $x\text{Na}_2\text{S} + (1-x)\text{P}_2\text{S}_5$ ($0.50 \leq x \leq 0.67$), which were prepared through mechanical milling. Their investigation focused on analyzing the short-range structures in glasses/glass-ceramics.

In this investigation, the melt-quenching technique was used to prepare glass samples with the composition of $x\text{Na}_2\text{S} + (100-x)\text{P}_2\text{S}_5$ ($40 \leq x \leq 55$) and applied heat treatment to convert them into glass-ceramics. The deliberate incorporation of an air + argon atmosphere during the glass preparation process was undertaken to introduce oxygen at localized sites within these glasses. This study offers an examination of the influence of occupied oxygens at specific sites on structural behaviour, electrical conductivity and band gap. Furthermore, the relationship between morphological effects and electrical conductivity is also discussed in order to support the findings.

EXPERIMENTAL

The glass-ceramics consisting of $x\text{Na}_2\text{S}-(100-x)\text{P}_2\text{S}_5$ ($40 \leq x \leq 55$) were synthesized through the melt-quench technique. Reagent-grade of $\text{Na}_2\text{S} \cdot 9\text{H}_2\text{O}$ (Sigma Aldrich, 99.9%) and P_2S_5 (Sigma Aldrich, 99%) crystalline powders were used as the starting materials. For each glass composition, the requisite amounts of chemicals, according to their stoichiometric ratios, were initially ground for 10 min with agate mortar and pestle under benzene medium. The powder mixtures were then placed into graphite crucible and melted at 700°C with a heating rate of $5^\circ/\text{min}$ under the flowing argon atmosphere. After maintaining the molten mass at 700°C for 15 min, it was rapidly quenched by copper plates. Subsequently, the as-prepared sample was ground in an agate mortar for 30 min and cold-pressed under 10 tons of pressure for 5 min to make pellets of (15 mm diameter and 2 mm thickness) dimensions. The glass-ceramics were obtained by subjecting the pellets to heat treatment at 350°C for 4 h with a heating rate of $5^\circ/\text{min}$ under an argon atmosphere. The X-ray diffraction (XRD) characterization was performed at room temperature using a PANalytical X'Pert PRO system with Ni-filter, where the incident X-ray wavelength was 1.54 \AA and the scan speed was $0.013^\circ/\text{min}$. The scan angle (2θ) ranged from 10 to 80° and the volume fractions of crystalline phases were determined using X-Pert High Score Plus software.

Absorption spectra of the prepared glass-ceramics were recorded with a Hitachi double-beam double-monochromator spectrophotometer (U-3900H) in the wavelength range of 190 nm to 900 nm. The grain size and morphology of the prepared glass-ceramics were examined using FE-SEM Quanta 200F. To enhance the conductivity measurements, both sides of all glass-ceramic samples were polished with emery paper and gold sputtered. Electrical conductivity measurements were conducted using ac impedance spectroscopy (Solatron 1260 Impedance/

gain phase analyzer) in the frequency range of 20 to 1×10^6 Hz in air at room temperature.

The bulk density of the glass-ceramic samples was determined by Archimedes' principle using toluene as an immersion liquid with a stable density of 0.866 g/cm^3 at room temperature.

The well known equation is given below:

$$\rho = \frac{m \text{ (g)}}{V \text{ (cc)}} \quad (1)$$

where ρ represents the density, m and V denote the mass and volume of the sample, respectively. The reported density values for the immersion liquid in this study were calculated as an average of a minimum of three independently measured values.

RESULTS AND DISCUSSION

XRD analysis: Fig. 1 illustrates the XRD pattern of glass-ceramics with $x = 40, 45, 50,$ and 55 mol% Na_2S . All the four samples display three phases, namely NaPO_3 (ICDD No. 00-011-0648), $\text{Na}_2\text{S}_2\text{O}_3$ (ICDD No. 00-011-0648) and Na_3PS_4 (ICDD No. 01-081-1472). The orthorhombic crystal structure characterizes NaPO_3 and $\text{Na}_2\text{S}_2\text{O}_3$ phases, while the Na_3PS_4 phase exhibits a tetragonal crystal structure. The presence of oxide phases suggests the possibility that some amount of Na_2S may have converted into Na_2O during the grinding and melting processes involved in the glass preparation. The calculated volume fractions of these phases are presented in Table-1.

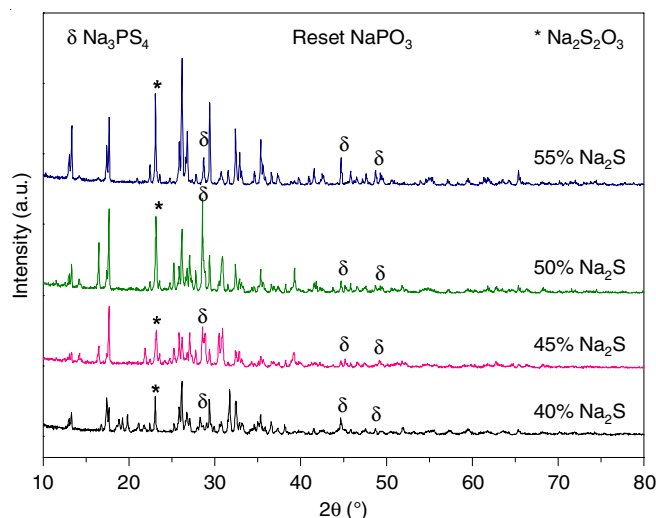


Fig. 1. XRD pattern of glass ceramics for $x = 40, 45, 50$ and 55 mol % Na_2S

The XRD pattern indicates a trend where, with an increase in the modifier (Na_2S) content, the volume fraction of the NaPO_3 phase decreases, while simultaneously, the fractions of $\text{Na}_2\text{S}_2\text{O}_3$ and Na_3PS_4 phases increase. This observation aligns with the findings reported by Hayashi *et al.* [17], who observed a similar Na_3PS_4 phase with a tetragonal crystal structure in the $\text{Na}_2\text{S}-\text{P}_2\text{S}_5$ system using a mechano-chemical technique.

Density: Fig. 2 depicts the density variation for the prepared glass ceramics with $x = 40, 45, 50$ and 55 mol% Na_2S . Table-1 also confirmed that with an increase in the Na_2S content, the density correspondingly increases. Typically, in alkali phosphate glasses, the addition of sodium sulfide or sodium oxide serves

TABLE-1
GLASS COMPOSITION (mol %), DENSITY VALUES, BAND GAP, BULK RESISTANCE, IONIC CONDUCTIVITY AND VOLUME FRACTIONS OF SODIUM PHOSPHATE GLASS-CERAMICS

| Glass composition (mol %) | | Density, ρ (g/cc) | Band gap (eV) | Bulk resistance (Ω) $\times 10^3$ | Ionic conductivity (S/cm) $\times 10^{-6}$ | Volume fractions | | |
|---------------------------|-------------------------------|------------------------|---------------|--|--|-------------------|---|---------------------------------|
| Na ₂ S | P ₂ S ₅ | | | | | NaPO ₃ | Na ₂ S ₂ O ₃ | Na ₃ PS ₄ |
| 40 | 60 | 2.24 | 3.60 | 118.2 | 1.2 | 85 | 7 | 8 |
| 45 | 55 | 2.29 | 3.48 | 72.8 | 1.8 | 81 | 9 | 10 |
| 50 | 50 | 2.33 | 3.35 | 6.11 | 20 | 74 | 12 | 14 |
| 55 | 45 | 2.35 | 2.99 | 1.84 | 60 | 69 | 16 | 15 |

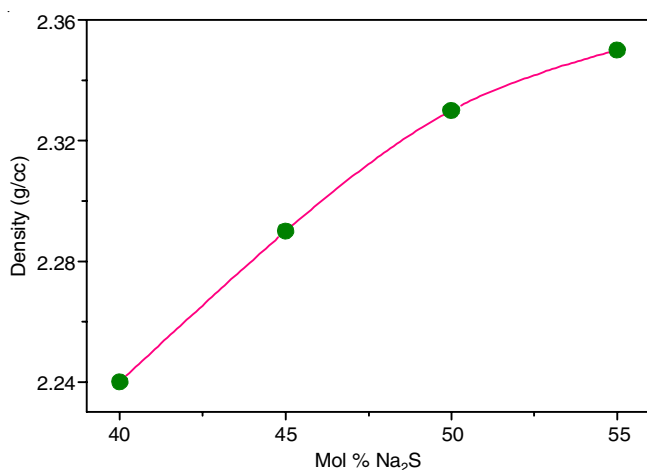


Fig. 2. Variation in density for $x = 40, 45, 50$ and 55 mol % Na₂S glass-ceramics

as a modifier. The introduction of alkali sulfide or oxide typically results in the formation of non-bridging sulfur or oxygen ions (NBOs or NBOs) within the phosphate matrix. These ions signify broken bonds in the network. Sodium ions are bonded to the surrounding sulfurs or oxygens by bonds that are ionic and weaker compared to the P-S or P-O bond. As a consequence, the structure of sodium phosphate glass is weaker than that of other phosphate glasses. Therefore, an increase in Na₂S or Na₂O content in the glass-ceramics contributes to an elevated number of non-bridging sulfur or non-bridging oxygen ions, compacting the local structure of the glass-ceramics and potentially leading to an increase in density [18].

All the samples in this investigation exhibit higher density in comparison to the previously reported densities of solid electrolytes based on Li₂S-P₂S₅ [19]. Consequently, the present samples have the potential for use as electrolytes in Na-ion batteries, offering a cost-effective alternative to Li₂S-P₂S₅ based batteries with comparable or improved performance.

UV-visible analysis: Fig. 3 presents Tauc's plot for the prepared glass ceramics. The investigation of optical absorption is valuable for comprehending optically induced transitions and the optical band gaps of materials. The band gap was determined from the Tauc plot [20] using the following relation:

$$\alpha h\nu = A(h\nu - E_g)^n \quad (2)$$

where E_g represents the band gap corresponding to a specific transition occurring in the sample; A is a constant; ν is the transition frequency and the exponent 'n' characterizes the nature of the band transition [21]. The direct band gap energy for the glass-ceramic sample was derived from the plot of $(\alpha h\nu)^2$ versus

the photon energy ($h\nu$) with extrapolation of the linear portion of the curve to $(\alpha h\nu)^2 = 0$ as depicted in Fig. 3.

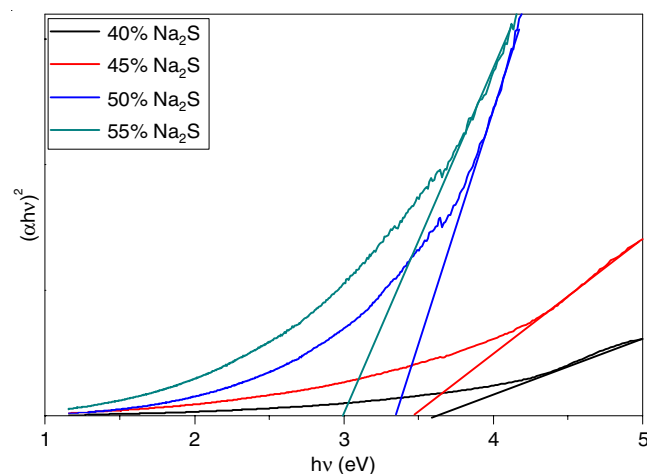


Fig. 3. Tauc's plot for $x = 40, 45, 50$ and 55 mol % Na₂S glass ceramics

Initially, the parent glass samples exhibited band gaps in the range of 4-5 eV. After heat treatment, the glass transformed into glass-ceramics and the band gap decreased from 4-5 eV to 2.99-3.60 eV as shown in Table-1. The higher content of modifier in the phosphate network was found to disrupt bridging oxygens (BOs) or bridging sulfurs (BSs) leading to the formation of non-bridging oxygens (NBOs) or non-bridging sulfurs (NBSs) [22].

Fig. 3 reveals that as modifier content (Na₂S) in the glass-ceramic increases, the band gap decreases from 3.60 eV to 2.99 eV. This phenomenon is attributed to the production of two NBOs or two NBSs per Na₂O or Na₂S molecule, with Na⁺ ions occupying sites in the phosphate matrix. Essentially, the negative charges on the NBSs or NBOs have a higher magnitude compared to BOs or BSs, causing them to move to the top of the valence band and resulting in a reduction of the optical band gap [23]. This observation is supported by Stenz *et al.* [24], who reported that the absorption edge in oxide glasses corresponds to the transition of an electron belonging to oxygen in an excited state. The weaker the binding of these electrons, the easier the absorption occurs.

Ionic conductivity: Impedance plots typically reveal distinct semicircles, where the high-frequency semicircle corresponds to the grain interior (bulk) impedance, the intermediate range frequency semicircle represents the grain-boundary impedance and the low-frequency semicircle arises from polarization effects due to charge carrier blocking at the electrodes.

However, in the prepared samples, only the bulk contribution was observed. The bulk (grain) properties of the material arise from the parallel combination of bulk resistance (R_b) and bulk capacitance (C_b). The value of bulk resistance (R_b) at ambient temperature has been determined from the intercept of semi-circular arc on the real axis (Z') and is provided in Table-1.

The obtained resistances are used to calculate conductivity using the following relation:

$$\sigma = \frac{l}{RA} \quad (3)$$

where l represents the thickness of pellet; R is the bulk resistance and A denotes the cross-sectional area of pellet.

The prepared samples with $x = 40$ and $x = 45$ exhibited ionic conductivity in the range of $1.2-1.8 \times 10^{-6} \text{ S cm}^{-1}$, while samples $x = 50$ and $x = 55$ demonstrated ionic conductivity in the range of $0.2-0.6 \times 10^{-4} \text{ S cm}^{-1}$. These results clearly indicate a dependence of ionic conductivity on the compositions. The observed increase in ionic conductivity with the increase in

Na_2S or Na_2O content suggests that in glass ceramics, the concentration of positively charged ions (Na^+) increases, serving as the primary source of conduction. Furthermore, the data in Table-1 suggests that an increase in Na_2S content leads to an increase in sulfide-based phases. Sulfide systems generally exhibit high polarizabilities of sulfide ions, contributing to enhanced ionic conductivity in the system [25].

Moreover, samples with $x = 50$ and $x = 55$ compositions have ionic conductivity in the range of earlier reported exhibit ionic conductivity within the range of values reported earlier [17] for the same $x\text{Na}_2\text{S}-(100-x)\text{P}_2\text{S}_5$ system at $x = 75$. Therefore, these samples could be utilized as solid electrolytes in Na-ion batteries at room temperature. Further analysis, including cyclic voltammetry (CV) measurements, energy density assessments, *etc.* is necessary to evaluate the suitability of these samples for use in the Na-ion batteries.

Micro-structural analysis: Fig. 4 displays the fractured surface of FE-SEM micrographs for $x = 40, 45, 50$ and 55 glass-ceramics. All micrographs distinctly revealed two morphologies

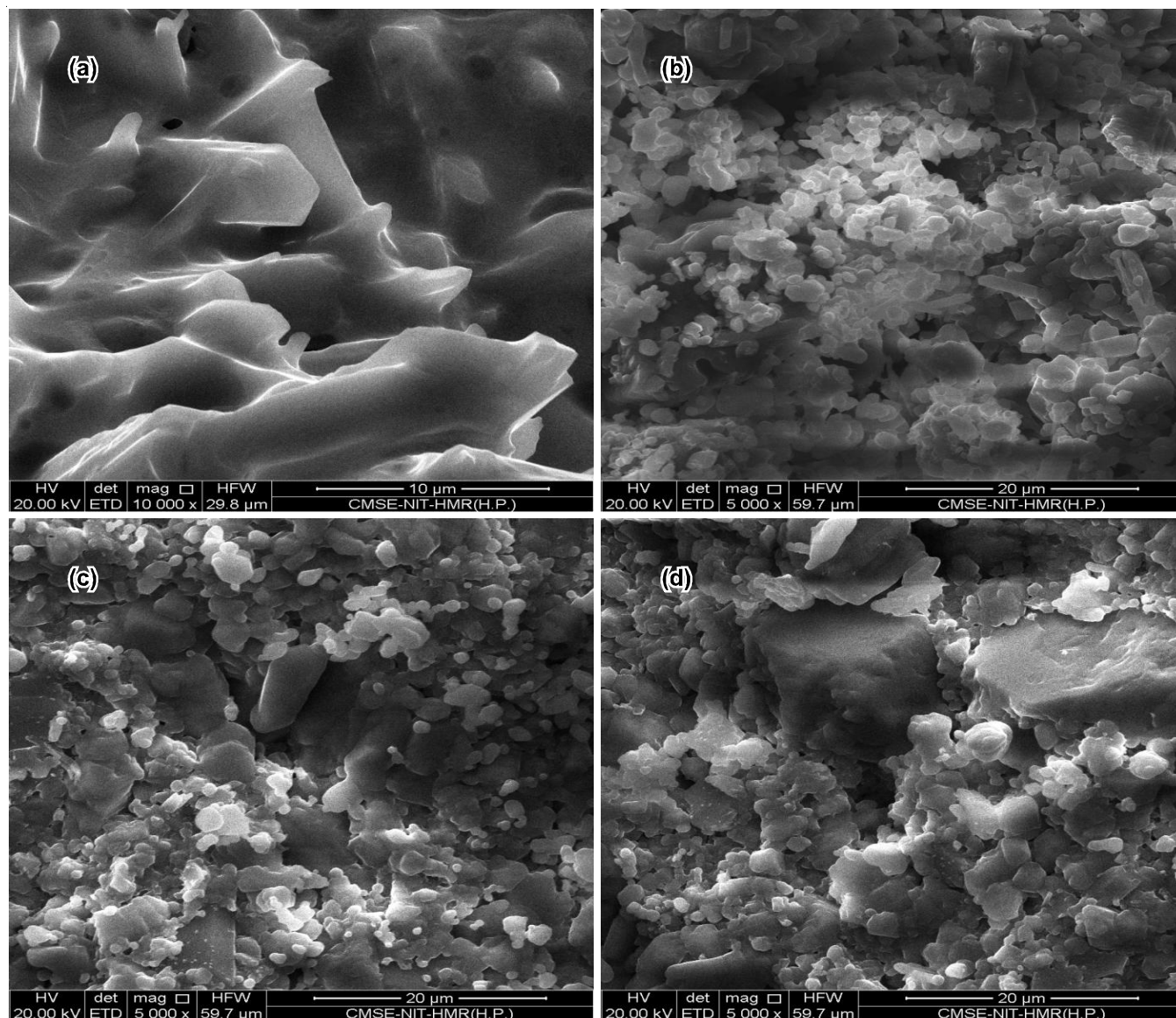


Fig. 4. Fractured surface FE-SEM micrographs for $x = 40, 45, 50$ and 55 glass ceramics

viz. one of a densified glassy phase and the other of a crystalline phase. In Fig. 4a, the glass-ceramics comprise a network of interlocking elongated and prismatic crystals embedded in a glassy phase. Remarkably, sample $x = 40$ was found to be highly unstable, reacting with atmospheric moisture during measurements and appearing melted. Fig. 4b exhibits some porosity in comparison to Fig. 4c-d. Fig. 4c-d display very dense and well-integrated contacts between the glassy and granular crystals, supporting the higher density values provided in Table-1.

Samples for $x = 45$, 50 and $x = 55$ exhibit clear grain and grain boundary features emerging from the glassy matrix. The crystalline part observed in these micrographs corresponds to Na_3PS_4 and $\text{Na}_2\text{S}_2\text{O}_3$ phases, while the glassy phase corresponds to the NaPO_3 phase, as also identified in the XRD analysis. The morphological features observed in the present samples indicate better intimate contact when compared to morphologies reported earlier [20] for $\text{Li}_2\text{S-P}_2\text{S}_5$ based solid electrolytes.

Conclusion

Glass-ceramics with the composition of $x\text{Na}_2\text{S} + (100 - x)\text{P}_2\text{S}_5$ ($40 \leq x \leq 55$) were synthesized using the melt-quenching technique. The XRD patterns of the synthesized glass-ceramics revealed the presence of three phases *viz.* NaPO_3 , $\text{Na}_2\text{S}_2\text{O}_3$ and Na_3PS_4 , exhibiting orthorhombic and tetragonal crystal structures, respectively. The measured densities of the samples fell within the range of 2.24-2.35 g/cc, surpassing those of Li_2S -based solid electrolytes. The band gap values ranged from 2.99 to 3.60 eV, indicating a decrease in band gaps with an increase in Na_2S content (modifier), contributing to enhanced ionic conductivity. At ambient temperature, the samples with $x = 50$ and 55 demonstrated a conductivity on the order of $10^{-4} \text{ S cm}^{-1}$. The FE-SEM micrographs exhibited a combination of glassy phases along with well-developed and dense crystals. The present samples exhibited comparable ionic conductivity and higher densities compared to Li_2S -based solid electrolytes commonly used in portable devices. Consequently, these glass-ceramics have the potential for application in Na-ion batteries, serving as a viable and cost-effective substitute for $\text{Li}_2\text{S-P}_2\text{S}_5$ based batteries.

CONFLICT OF INTEREST

The authors declare that there is no conflict of interests regarding the publication of this article.

REFERENCES

1. X. Rong, Y. Lu, X. Qi, Q. Zhou, W. Kong and K. Tang, *Energy Storage Sci. Technol.*, **9**, 515 (2020); <https://doi.org/10.19799/j.cnki.2095-4239.2020.0054>
2. M. Nishijima, I.D. Gocheva, S. Okada, T. Doi, J.I. Yamaki and T. Nishida, *J. Power Sources*, **190**, 558 (2009); <https://doi.org/10.1016/j.jpowsour.2009.01.051>

3. A. Rudola, A.J.T. Rennie, R. Heap, S.S. Meysami, A. Lowbridge, F. Mazzali, R. Sayers, C.J. Wright and J. Barker, *J. Mater. Chem. A Mater. Energy Sustain.*, **9**, 8279 (2021); <https://doi.org/10.1039/D1TA00376C>
4. P. Sharma, P.K. Jha, P.K. Diwan and O.P. Pandey, *J. Non-Cryst. Solids*, **477**, 31 (2017); <https://doi.org/10.1016/j.jnoncrysol.2017.09.046>
5. N. Kamaya, K. Homma, Y. Yamakawa, M. Hirayama, M. Yonemura, R. Kanno, T. Kamiyama, Y. Kato, S. Hama, K. Kawamoto and A. Mitsui, *Nat. Mater.*, **10**, 682 (2011); <https://doi.org/10.1038/nmat3066>
6. D. Larink, H. Eckert and S.W. Martin, *J. Phys. Chem. C*, **116**, 22698 (2012); <https://doi.org/10.1021/jp3068365>
7. Y.K. Startsev, A.A. Pronkin, I.A. Sokolov and I.V. Murin, *Glass Phys. Chem.*, **37**, 263 (2011); <https://doi.org/10.1134/S1087659611030138>
8. B.E. Francisco, C.M. Jones, S.H. Lee and C.R. Stoldt, *Appl. Phys. Lett.*, **100**, 103902 (2012); <https://doi.org/10.1063/1.3693521>
9. M. Tatsumisago and A. Hayashi, *Solid State Ion.*, **225**, 342 (2012); <https://doi.org/10.1016/j.ssi.2012.03.013>
10. M. Tatsumisago, T. Saito and T. Minami, *Chem. Lett.*, **30**, 790 (2001); <https://doi.org/10.1246/cl.2001.790>
11. F. Mizuno, A. Hayashi, K. Tadanaga and M. Tatsumisago, *Adv. Mater.*, **17**, 918 (2005); <https://doi.org/10.1002/adma.200401286>
12. A. Hayashi, K. Minami, S. Ujiie and M. Tatsumisago, *J. Non-Cryst. Solids*, **356**, 2670 (2010); <https://doi.org/10.1016/j.jnoncrysol.2010.04.048>
13. N. Ohta, K. Takada, L. Zhang, R. Ma, M. Osada and T. Sasaki, *Adv. Mater.*, **18**, 2226 (2006); <https://doi.org/10.1002/adma.200502604>
14. M. Tatsumisago and A. Hayashi, *Funct. Mater. Lett.*, **1**, 31 (2008); <https://doi.org/10.1142/S1793604708000071>
15. L. Zhao, T. Zhang, W. Li, T. Li, L. Zhang, X. Zhang and Z. Wang, *Engineering*, **24**, 172 (2023); <https://doi.org/10.1016/j.eng.2021.08.032>
16. S. Xu, H. Dong, D. Yang, C. Wu, Y. Yao, X. Rui, S. Chou and Y. Yu, *ACS Cent. Sci.*, **9**, 2012 (2023); <https://doi.org/10.1021/acscentsci.3c01022>
17. A. Hayashi, K. Noi, A. Sakuda and M. Tatsumisago, *Nat. Commun.*, **3**, 856 (2012); <https://doi.org/10.1038/ncomms1843>
18. S.S. Berbano, I. Seo, C.M. Bischoff, K.E. Schuller and S.W. Martin, *J. Non-Cryst. Solids*, **358**, 93 (2012); <https://doi.org/10.1016/j.jnoncrysol.2011.08.030>
19. P.K. Jha, O.P. Pandey and K. Singh, *J. Mol. Struct.*, **1083**, 278 (2015); <https://doi.org/10.1016/j.molstruc.2014.11.027>
20. A. Sakuda, A. Hayashi and M. Tatsumisago, *Sci. Rep.*, **3**, 2261 (2013); <https://doi.org/10.1038/srep02261>
21. V.M. Yogesh and V.S. Shrivastava, *Adv. Appl. Sci. Res.*, **2**, 295 (2011).
22. G. Kaur, M. Kumar, K. Singh and O.P. Pandey, *J. Non-Cryst. Solids*, **357**, 863 (2011).
23. J.A. Duffy, *Phys. Chem. Glasses*, **42**, 151 (2001).
24. D. Stenz, H.B. George and S.E. Feller, *Phys. Chem. Glasses*, **41**, 406 (2000).
25. R. Kanno and M. Murayama, *J. Electrochem. Soc.*, **148**, A742 (2001); <https://doi.org/10.1149/1.1379028>